

Multiparticle production in lepton-nucleus collisions and relativistic string models

D. J. Dean,^(1,2) M. Gyulassy,⁽³⁾ B. Müller,⁽⁴⁾ E. A. Remler,⁽⁵⁾ M. R. Strayer,⁽¹⁾
A. S. Umar,^(2,1) and J.-S. Wu,⁽¹⁾

⁽¹⁾Center for Computationally Intensive Physics, Physics Division,
Oak Ridge National Laboratory, Oak Ridge, Tennessee 37831

⁽²⁾Vanderbilt University, Department of Physics & Astronomy, Nashville, Tennessee 37235

⁽³⁾Nuclear Science Division, Lawrence Berkeley Laboratory, Berkeley, California 94720

⁽⁴⁾Department of Physics, Duke University, Durham, North Carolina 27706

⁽⁵⁾Department of Physics, College of William and Mary, Williamsburg, Virginia 23185

(Received 21 October 1991)

Nuclear attenuation of the leading ($x_f > 0$) hadron and the nuclear enhancement of target fragmentation ($x_f < 0$) hadrons in lepton-nucleus reactions are calculated via a (3+1)-dimensional string-parton model. A (1+1)-dimensional string model is used to investigate the dependence of rapidity distributions on the lepton energy loss, $\nu = 10\text{--}100$ GeV, the atomic number, $A = 1\text{--}200$, the effective string tension, $\kappa = 0.5\text{--}2$ GeV/fm, the string decay constant, $\tau_0 = 0.5\text{--}2$ fm/c, and the string flip cross section, $\sigma_{lq} = 0\text{--}30$ mb. The (3+1)-dimensional string-parton model includes inelastic final state cascading of produced hadrons in the nucleus. We show how the A dependence of hadronic production in lepton-nucleus collisions, especially in the $x_f < 0$ region, may be used to extract information on quark propagation and hadronization in nuclei.

PACS number(s): 24.85.+p, 25.30.-c

I. INTRODUCTION

The study of hadroproduction in deep inelastic lepton-nucleus reactions offers the possibility to investigate quark propagation in dense nuclear matter and the space-time evolution of hadronization [1]. The final state distribution of hadrons depends on the nonperturbative physics of strong interactions and presently can only be treated via phenomenological models. Beginning with the classic work of Artru [2], a successful phenomenology [3, 4] of hadronization has been developed based on relativistic string dynamics [5]. Recent work [6–9] has extended string model phenomenology to relativistic hadron-nucleus and nucleus-nucleus collisions. These models provide a tool for studying the complex evolution of hadronic matter in relativistic heavy-ion collisions.

The usefulness of relativistic string models stems from their covariant treatment of strongly interacting extended (hadronic) objects. The space-time scale of string interactions is controlled by an effective string tension, $\kappa \sim 0.5\text{--}2$ GeV/fm. This choice for the range of κ is discussed below. Covariant string breaking or splitting provides the mechanism leading to multiparticle production. A proper time decay constant, τ_0 , determines the mean breaking rate. For pointlike particles of transverse mass m_\perp , the uncertainty principle provides a natural scale, $\tau_0 \sim \hbar/m_\perp$. However for composite particles, τ_0 must be taken from fits to experimental data. In the following we investigate the range of values $\tau_0 \sim 0.5\text{--}1.0$ fm/c, and fit τ_0 from ℓp experimental data. String flip or quark-quark scattering and exchange processes provide a covariant mechanism leading to highly inelastic interactions. Since we are interested only in inelastic processes, these interaction cross sections are constrained to be less

than 30 mb, and should also be greater than 10 mb by the constituent quark model. Thus we vary the leading quark cross section $\sigma_{lq} \sim 10\text{--}30$ mb. We also note that our interaction mechanism does not carry any explicit color degrees of freedom. Therefore, cross sections for quark-nucleon interactions in which there is momentum exchange without color exchange, are buried in these effective cross sections.

The purpose of this paper is to extend the application of string phenomenology to hadroproduction in lepton-nucleus reactions. We concentrate on ℓA collisions because, unlike hadron or nuclear induced reactions, the dynamics of a single excited string with precisely constrained kinematics (ν, Q^2) can be studied. In this sense these collisions are the cleanest systems from which the phenomenological parameters can be deduced. Those parameters can then be used directly for applications of string models to pA and AA collisions. In [10] a greatly simplified analytic string model was applied to analyze data in the $x_f > 0.1$ region. In the present work we extend this analysis to the full x_f region utilizing the exclusive event capabilities of the complete dynamical string model. We first study the (1+1)-dimensional string model because of its numerical simplicity, and because it reveals clearly the sensitivity of the results to variations of the basic phenomenological parameters, $\kappa, \tau_0, \sigma_{lq}$. Then we apply the full (3+1)-dimensional string-parton model [8] which enables us to investigate the role of intranuclear cascading.

The importance of using the computationally more demanding 3+1 model is that secondary cascading of hadrons in conventional transport theories suffers from a basic ambiguity associated with defining the forma-

tion time of an extended object such as a hadron [11]. In particular, different constituents of hadrons may be produced at different times and thus the effect of cascading becomes strongly model dependent. The 3+1 string model overcomes this serious limitation with the assumption that inelastic interactions can occur via parton-parton scattering regardless of whether the current string configurations are in their lowest ground states or not. A high invariant-mass string fragment is thus able to suffer inelastic reactions as it decays to lower mass stringlets. The entire dynamics is governed by a few phenomenological string parameters. Furthermore, the 3+1 model is also suitable for studying the dynamical influence of $q\bar{q}$ pair production during the hadronization phase. Quarks are created as virtual pairs in the model, and take time to become on shell. Implementation of these processes will be described below.

String models are able to simulate successfully a number of key features of coherent QCD radiative processes. In perturbative QCD interactions between partons are believed to be mediated by multiple soft gluon exchanges which always lead to induced gluon bremsstrahlung. The remarkable property of this radiation is that the distribution of induced soft gluons is approximately uniform in rapidity and limited in transverse momentum, q_{\perp} , to the scale of the momentum transfer [12]. In contrast, for QED a uniform rapidity distribution only follows for hard processes [13]. When considering the energy loss of a quark as it traverses nuclear matter, the Landau-Pomeranchuk effect [14], must also be taken into account. This effect states that the formation length ℓ of a parton with transverse momentum k_{\perp} and rapidity y increases as $\ell \sim \cosh(y)/k_{\perp}$. This effect, together with the soft gluon bremsstrahlung, leads to an approximately constant energy loss per unit length [15]. Numerical estimates in [15] gave $dE/d\ell \sim 1-3$ GeV/fm. Therefore, the tension κ in string models can be thought of as essentially simulating the approximately constant energy loss of perturbative QCD. In this paper we will investigate the role κ plays in ℓA collisions over the representative range $\kappa \sim 0.5-2$ GeV/fm.

The role of κ as a mean energy loss of a quark in the nuclear medium, per unit distance traveled, becomes obvious when string flip interactions are taken into account [10]. As a string traverses matter composed of other stringlike configurations, the string flip mechanism leads to a series of reconnections that leave target strings with an energy $\kappa\lambda_s$, where λ_s is the string flip mean free path. After traversing a distance R , the incident string will have lost an amount of energy κR . This simple mechanism simulates an induced bremsstrahlung associated with soft gluon exchange in matter. We assume that κ is medium independent. All possible sources of quark energy loss are then combined in the product $\kappa\lambda_s$. In string models, we are not able to distinguish the various mechanisms which may contribute to the leading-quark energy loss. As emphasized also in [16], induced radiation is limited by the Landau-Pomeranchuk effect to gluons with $\cosh(y) < k_{\perp}R$. This is the basic physics that is responsible for asymptotic QCD factorization. The consistency of string models with QCD factorization is

important because without it the phenomenology would fail [10].

While incorporating the above features of perturbative dynamics, it is of course not obvious how accurately other important QCD properties are simulated. In this regard, it is especially remarkable that even subtle interference phenomena [17] such as the so-called ‘‘string effect’’ in three jet events [3] can be quantitatively reproduced by this simple classical phenomenology. The overall success of string models to reproduce quantitatively many observed features of multiparticle production in e^+e^- , e^-p , and pp is striking and has motivated the recent extensions of this model to eA , pA , and AA reactions [6–10].

For application to lepton-nucleus reactions the string flip interaction provides a mechanism for the interaction of the leading quark (the quark which is struck by the incoming lepton) with nuclear matter. Here, the leading quark (string end point) may reconnect successively to different diquark string ends in the nucleus. This exchange of string end points leads to a configuration of various excited strings

$$\begin{aligned} \gamma^* A \rightarrow & [(qq)_0q_1] + [(qq)_1q_2] + \cdots \\ & + [(qq)_{n-1}q_n] + [(qq)_nq_0] + (A - n + 1). \end{aligned} \quad (1)$$

Eventually the $n + 1$ strings fragment into secondary hadrons. The baryons left in the wake of the leading quark are in an excited state with energy on the order $\kappa\lambda_s$, where λ_s is the mean free path of the leading quark in the nucleus. The baryonic stringlets are thus excited to an energy of only about 2 GeV when the quark scattering cross section is taken to be $\sigma_{Iq} = 30$ mb. As it was pointed out in Ref. [10], decays of these target baryonic strings therefore do not contribute to the $x_f > 0$ region where nuclear attenuation has been observed [18]. This suggested that most of the nuclear suppression at $x_f > 0$ of leading particles could be due to the energy loss of the quark as it propagates through the nucleus and not to any intranuclear cascading of the secondaries.

To test the above picture in more detail we utilize the full (3+1)-dimensional string model, which includes both the interaction of the leading quark as well as final state cascading in the target nucleus. This is the primary aim of this paper. In Sec. II, we discuss first a (1+1)-dimensional string model, and then turn to the (3+1)-dimensional string-parton model of Ref. [8]. In Sec. III the numerical results are compared to data on $\mu-p$ and $\mu-A$ collisions. A discussion emphasizing the necessity of studying the global nuclear dependence in both $x_f < 0$ and $x_f > 0$ regions to deconvolute the effects of leading quark interactions in matter and secondary particle cascading is presented in Sec. IV.

II. RELATIVISTIC STRINGS

A. (1+1)-dimensional Nambu strings

A (1+1)-dimensional relativistic string satisfies the following equations of motion for one of the string end points ($c = \hbar = 1$):

$$\frac{dx}{dt} = \pm 1, \quad \frac{dp}{dt} = \pm \kappa. \quad (2)$$

The plus (minus) sign in the dx/dt equation corresponds to a right (left) moving end point, while the plus (minus) sign in the momentum equation refers to the left (right) end of the string. An example of a (1+1)-dimensional string is shown in Fig. 1. The string is shown in its light cone coordinates, where the end points sweep out the rectangular box as they move in time. The string is pictured at time t_i , when its end points are at positions α and β , and the string length is L . We may determine the mass and momentum of this string geometrically. Note that $s_1 + s_2 = x_i - x_{i-1}$ and $s_2 - s_1 = t_i - t_{i-1}$. Solving for s_1 and s_2 , we obtain

$$s_{1,2} = [(x_i - x_{i-1}) \mp (t_i - t_{i-1})]/2. \quad (3)$$

Therefore, $b = \sqrt{2}s_2$ and $a = \sqrt{2}s_1$, and the area of the rectangle is given by $A = ab = [(x_i - x_{i-1})^2 - (t_i - t_{i-1})^2]/2$. We can relate this area to the mass of the string by calculating the energy and momentum of the string at time t_i . In this case the end point at β carries no momentum since it is at a turning point. The momentum of end point α is given by the accumulation of momentum from t_{i-1} to t_i ,

$$P_\alpha(t_i) = \kappa \int_{t_{i-1}}^{t_i} dt = \kappa(t_i - t_{i-1}). \quad (4)$$

Since the end points are massless, $E_\alpha = |P_\alpha|$. The segment of string between the end points carries no momentum in 1+1 dimensions, but it does have an energy associated with its length, $E_s = \kappa L = \kappa[(x_i - x_{i-1}) - (t_i - t_{i-1})]$, and therefore the mass of the system is given by

$$m^2 = E^2 - p^2 = (E_s + E_\alpha)^2 - P_\alpha^2 = 2\kappa^2 A, \quad (5)$$

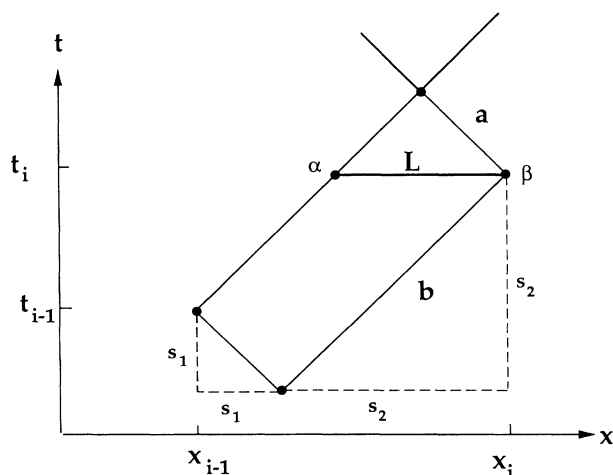


FIG. 1. The motion of the quarks of a (1+1)-dimensional string is shown. The string is pictured at time t_i , when its end points are at positions α and β , and the string length is L . Quark turning points are at positions x_i and x_{i-1} . The geometrical quantities s_1 , s_2 , a , and b are discussed in the text.

where $E = E_s + E_\alpha$ and $p = P_\alpha$. We also define the light cone momenta as $p^+ = (E + p)$ and $p^- = (E - p)$, with $m^2 = p^+ p^-$, and the lengths of the sides of the rectangle in these variables become $a = p^-/\sqrt{2}\kappa$ and $b = p^+/\sqrt{2}\kappa$.

The motion of (1+1)-dimensional strings, which may be followed using Eqs. (2), is supplemented by an interaction mechanism and a decay law. We use the string flip mechanism for interactions in the (1+1)-dimensional model [10]. This interaction leads to excited strings which are allowed to decay by breaking until they reach a predefined minimum mass. Each string may only decay into segments whose masses are above this cutoff mass. The minimum masses are $M_q = 0.28$ GeV for the meson strings and $M_{qq} = 0.94$ GeV for baryon strings. The choice for the decay point is based on the invariant area decay law [6–8], in which the probability \mathcal{P} for a small segment of string to decay is a function of the invariant area ΔA that the piece sweeps out as it propagates, $\mathcal{P} = 1 - \exp(-\Lambda \Delta A)$.

The decay constant Λ may also be expressed in terms of a proper time interval for decay, $\Lambda = 1/\tau_0^2$, where $\tau_0 \approx 1$ fm/c. This simple decay law, combined with the string dynamics, produces many of the general features observed in high-energy fragmentation [3, 6, 8, 19].

Application of the (1+1)-dimensional model to μ - A collisions involves the following assumptions. We start with a string at rest and give a large energy-momentum transfer to one of the quarks so that the string is excited to a definite invariant mass. The invariant quantities of this process are the variables Q^2 , which is the invariant mass squared of the virtual photon, and ν , which is the energy transfer to the quark in the nucleon rest frame. The positive and negative light cone momenta of the leading string after the four-momentum transfer are given by

$$p^\pm = M_n + \nu \pm \sqrt{\nu^2 + Q^2}, \quad (6)$$

where M_n is the nucleon rest mass. Once these initial conditions are established, the nucleon string propagates and can exchange its diquark with another target nucleon. String flip must not result in particles whose masses are below the cutoff masses assigned for mesons and baryons. As the excited quark moves through the nucleus, a random fraction of a nucleon mass is added to the leading quark string after it propagates one mean free path.

Since the virtual photon may interact with any nucleon, the struck parton interacts with only a fraction of the nucleus. We have simulated this effect in the 1+1 model by allowing the initially excited parton to travel some average distance in the nucleus. Thus, we consider a uniform distribution of A nucleons within a sphere of radius $R = 1.1A^{1/3}$. The average distance through which the struck parton moves in a nucleus is given by $0.75R$.

B. (3+1)-dimensional string-parton model

In this section we give a brief outline of the dynamical string-parton model developed for simulating the physics of strongly interacting particles with finite extent. The

model incorporates the relativistic strings in their most general form with massless end points. The dynamical calculations are carried out in three-dimensional space with no symmetry assumptions. An ensemble of strings with different end-point dynamics is used to reproduce the valence quark structure functions. Further details of the model are given in Ref. [8].

The action of a relativistic string is constructed in analogy with the action of a free particle. While the free particle action is proportional to the length of its world line, the string action is proportional to the invariant area swept by the string. The string is defined to be a finite curve in space which sweeps out a hypersurface in four-dimensional space-time. The two-dimensional surface can be parametrized in terms of the general coordinates τ and s as $x^\mu(\tau, s)$. For a two-dimensional surface embedded in four-dimensional space-time the area element is [5]

$$dA = \left[\left(\frac{\partial x^\mu}{\partial s} \frac{\partial x_\mu}{\partial \tau} \right)^2 - \left(\frac{\partial x^\mu}{\partial s} \frac{\partial x_\mu}{\partial s} \right) \left(\frac{\partial x^\nu}{\partial \tau} \frac{\partial x_\nu}{\partial \tau} \right) \right]^{\frac{1}{2}} ds d\tau$$

which is used to define the string action as

$$S = -\kappa \int dA. \quad (7)$$

The time over which the action is to be considered is defined by an initial time τ_i and a final time τ_f . The string ends are defined to be $s = 0$ and $s = S$, and κS represents the accumulative energy of the string from its zero end point to any other point along the string. Thus, the total energy of the string is κS . The initial and final configurations of the string will be those seen by a definite observer at a given instant of time in his Lorentz frame. This action is invariant under general string coordinate transformations and satisfies energy-momentum conservation.

General equations of motion and the boundary conditions are obtained by small variations of the surface that joins the initial and final configurations of the string. Due to the arbitrariness of the parametrization of the surface swept by the string, we can choose additional coordinate conditions (Virasoro gauge conditions) which simplify the equations of motion. We work with the *orthonormal* parametrization

$$\begin{aligned} \frac{\partial x^\mu}{\partial s} \frac{\partial x_\mu}{\partial \tau} &= 0, \\ \left(\frac{\partial x^\mu}{\partial \tau} \right)^2 + \left(\frac{\partial x^\mu}{\partial s} \right)^2 &= 0. \end{aligned} \quad (8)$$

The equations of motion are given by [8]

$$\frac{\partial^2 x^\mu}{\partial \tau^2} - \frac{\partial^2 x^\mu}{\partial s^2} = 0, \quad (9)$$

with associated boundary conditions

$$\frac{\partial x^\mu(\tau, 0)}{\partial s} = \frac{\partial x^\mu(\tau, S)}{\partial s} = 0. \quad (10)$$

In the following we choose the coordinates such that $x^0(\tau, s) = \tau = ct$.

The solution of Eq. (9), subject to the above coordinate conditions and the first of the conditions in Eq. (10), gives

$$x^\mu(\tau, s) = \frac{1}{2} [y^\mu(\tau + s) + y^\mu(\tau - s)], \quad (11)$$

where we have defined $y^\mu(t) \equiv x^\mu(t, 0)$, which is the trajectory of a single end point, also called the *directrix*. This indicates that the entire string can be constructed from the knowledge of the trajectory of a single end point. The application of the second boundary condition in Eq. (10) results in the end point periodicity equation

$$y^\mu(\tau + S) = y^\mu(\tau - S) + \frac{2P^\mu}{\kappa}, \quad (12)$$

where P^μ is the total four-momentum of the string, and is given by

$$P^\mu = \kappa \int_0^S ds \frac{\partial x^\mu}{\partial \tau}. \quad (13)$$

Details of string construction and motion can be found in Ref. [8].

We have shown in Ref. [8] that different dynamical states of motion of the strings give rise to different fractional momentum distributions of the string end points, which are identified as massless partons. An ensemble average of different dynamical states of the strings is used to reproduce the valence quark structure function of the proton. Interactions in the (3+1)-dimensional model have been described in detail elsewhere [8]. Here we briefly summarize our approach. We allow for parton scattering of the string end points using a phenomenological ($u+t$)-channel scattering matrix element, and quark exchange. This marriage of the strings and partons has led to the development of the string-parton model, a fully dynamical, (3+1)-dimensional simulation [8].

An important aspect of the string-parton model is capable of producing particles with finite transverse momentum. In the (1+1)-dimensional case, there is no mechanism to create transverse momentum, and this results in one of the major differences between the two calculations. The quark and the antiquark of the created pair could carry equal and opposite nonvanishing transverse momenta. This source of transverse momenta will primarily contribute to the low momentum (approximately $p_T \leq 1.0$ GeV) part of the total transverse momentum distribution. In the absence of any fundamental calculations, we choose to parametrize the transverse momentum assignment with a simple exponential distribution function

$$f(p_T) p_T dp_T \propto e^{-\alpha p_T} p_T dp_T. \quad (14)$$

We also take into consideration the cutoff masses mentioned above. The created quarks are initially virtual and become on shell by absorbing energy from the string, thereby simulating the Landau-Pomeranchuk effect. In previous work, those strings with virtual quarks were not

allowed to interact with other strings [8]. This restriction has been removed in this work. The virtual quarks may not interact until they become real; however, other quarks on the string are now allowed to scatter as the string propagates through the nucleus, provided that interactions do not violate overall energy-momentum conservation.

The string-parton model has been applied to μ - A collisions as follows. A nucleus of nucleonlike strings, each string having the correct parton distribution and mass of 0.94 GeV, is generated. This is accomplished by using a spatial Fermi density distribution for the nucleus. The muon is allowed to interact with any of the nucleons in the target. Using the condition of massless string end points, we may calculate the value of q_z from energy-momentum conservation:

$$q_z = -k_z + \sqrt{k_z^2 + \nu(\nu + 2k_0)}, \quad (15)$$

where k is the four-momentum of the quark before it absorbs the photon's energy. Thus Q^2 and $x_{Bj} = Q^2/2M_n\nu$ are readily calculable, and any experimental cuts on these variables may be easily taken into account. The nucleus is then time evolved until all hard interactions and decays have taken place.

III. CALCULATIONS

A. Muon-proton deep-inelastic scattering

Before presenting μ - A results, we first consider μ - p experimental Feynman- x distributions, at an incident muon energy of 280 GeV [20], in order to fit the string parameters. Distributions were measured with an average energy transfer of $\langle \nu \rangle = 71$ GeV in the laboratory frame, and $Q^2 > 4$ GeV². Using the (1+1)-dimensional model, with $Q^2 = 4$ GeV², we have found that when $\kappa\tau_0 = 0.88$ GeV/c the model gives a reasonable representation of the experimental data. Our results are shown in Fig. 2, where Feynman x is defined as $x_f = 2p_3/W$. Here, p_3 is the momentum measured parallel to the virtual photon direction and $W^2 = M_n^2 + 2M_n\nu - Q^2$. Figure 2 shows the results of the 1+1 model for all hadrons (curve 3) and baryons (curve 4). The total hadronic production is given by summing up the appropriate experimental data and multiplying by factors to take into account unmeasured neutral hadron production. Thus, the filled circles represent the total hadronic distribution which is given by $1.5(\pi^+ + \pi^-) + 2p + 2(K^+ + K^-)$, where the experimental distributions are given individually for π^+ , π^- , K^+ , K^- , and p . Total hadron production is presented in Fig. 2 by the filled circles. Nucleon production is shown by the open circles, and is equal to twice the proton experimental data. Note that nucleon data at $x_f > 0$ are believed to be a result of diquark production during flux-tube decay, and are not treated in the present model. Based on these results, we will use $\kappa = 0.88$ GeV/fm, and $\tau_0 = 1.0$ fm/c as our standard parameter set in the 1+1 model.

We can also adjust the parameters of the (3+1)-dimensional model to reproduce the μ - p data. We choose

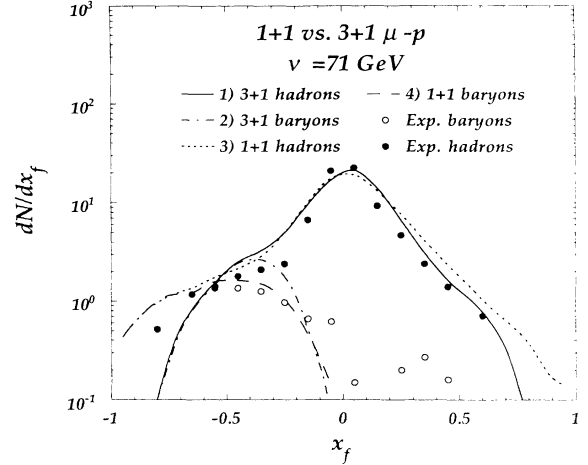


FIG. 2. Feynman- x distributions are shown for μ - p deep-inelastic scattering at 280 GeV [20] experimental data for $\nu = 71$ GeV. Total nucleon production, which is twice the proton data, is shown by opened circles, and total hadron production, which is given by $1.5(\pi^+ + \pi^-) + 2p + 2(K^+ + K^-)$ when we take into account the neutrals, is indicated by the filled circles. 1+1 model calculations with $Q^2 = 4$ GeV², $\kappa = 0.88$ GeV/fm, and $\tau_0 = 1.0$ fm/c reproduce the data for all hadrons (curve 3) and baryons (curve 4). 3+1 fits for $Q^2 > 4$ GeV², $\kappa = 0.88$ GeV/fm, and $\tau_0 = 0.5$ fm/c are also presented for all hadrons (curve 1) and baryons (curve 2).

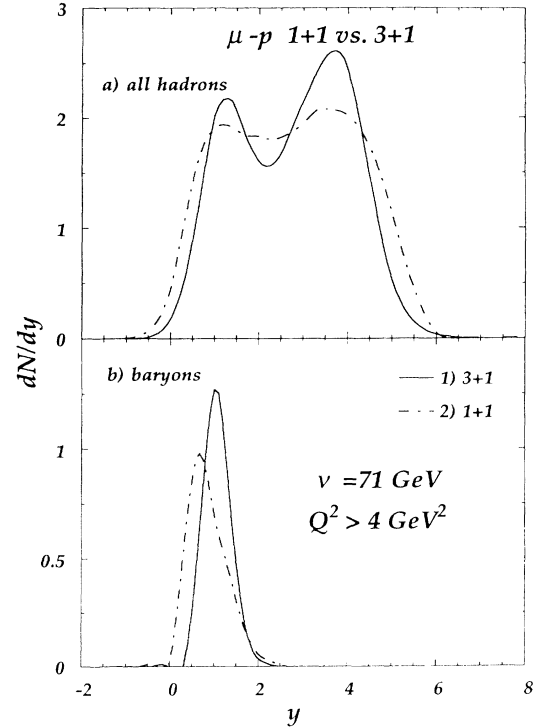


FIG. 3. Calculated μ - p rapidity distributions at $\nu = 71$ GeV for all produced particles using the same parameters as in Fig. 2. We show the 3+1 model production in curve (1), and the 1+1 model calculation in curve (2). Rapidity distributions are shown for (a) all hadrons and (b) for all baryons.

$\kappa = 0.88$ fm/c and $\tau_0 = 0.5$ fm/c. The agreement is shown in Fig. 2 for all hadrons (curve 1) and baryons (curve 2). The difference in τ_0 arises from the transverse momentum production mechanism present in the (3+1)-dimensional calculations. This process has a tendency to require an increase in the bare decay rate since some time is required for a created virtual quark pair to become on shell. Note also that the (3+1)-dimensional model does a better job of fitting the $x_f > 0$ total hadron data, but gives a narrower x_f distribution for the nucleons in the $x_f < 0$ region. If transverse momentum is turned off in the 3+1 model, the resulting curve (not shown) is almost the same as the 1+1 case.

It should also be noted that the 3+1 model does not require Q^2 to be specified on input. The 3+1 model gives a $\langle Q^2 \rangle = 11.5$ GeV², which is consistent with the experimental value given in Ref. [20]. We have checked that a variation of Q^2 in the 1+1 calculations causes no significant differences in the various distributions. With this choice of parameters for the 1+1 and 3+1 models, we have also calculated the rapidity distributions dN/dy , where $y = \ln(p^+/p^-)/2$, as shown in Fig. 3. We show in Fig. 3(a) the total hadron rapidity distributions, and in Fig. 3(b) we show the baryon distributions. The 3+1 model gives rise to a more forward-shifted nucleon distribution, and a less broad meson peak. This behavior is due to the transverse momentum production, and is a

characteristic difference between the 1+1 and 3+1 models. Average multiplicities in the two calculations differ by no more than 4% overall.

B. (1+1)-dimensional lepton-nucleus deep-inelastic scattering

Using the (1+1)-dimensional string flip model, we have calculated rapidity distributions while varying the parameters κ , τ_0 , and σ_{lq} . We have also investigated the ν and A dependences of the distributions. In these calculations, except where indicated, we have set $Q^2 = 4$ GeV², $\sigma_{lq} = 20$ mb, and we use a ⁶³Cu nucleus.

Figure 4 indicates how the rapidity distribution, dN/dy , varies with ν for $\tau_0 = 1.0$ fm/c, $\kappa = 0.88$ GeV/fm, and $\nu = 11, 60$, and 100 GeV. Notice that a rapidity plateau develops as one increases the energy, while the rapidity distributions in the region $y < 2$ remain virtually unchanged. Also note that the baryon distribution is shifted to slightly lower rapidity as ν is increased. This shows the limited ability of the nucleus to absorb energy from the leading quark. Furthermore, the mass distributions dm/dy , which are not shown, indicate that there is a great deal of mass in $0 < y < 2$. Much of this mass arises from the target nucleons that have been excited in the wake of the high-energy parton. Figure 5 shows how the decay parameter, τ_0 , affects the matter distribution at a fixed energy, $\nu = 60$ GeV,

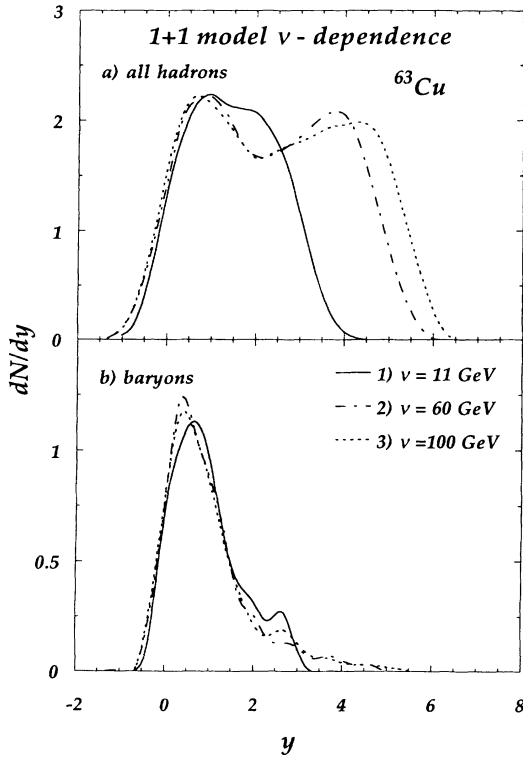


FIG. 4. The ν dependence of rapidity distributions calculated with the 1+1 model for $A = 63$, $Q^2 = 4$ GeV², $\kappa = 0.88$ GeV/fm, and $\tau_0 = 1.0$ fm/c. Calculations were performed at $\nu = 11$ GeV (curve 1), $\nu = 60$ GeV (curve 2), and $\nu = 100$ GeV (curve 3), and are shown for (a) all hadrons and (b) all baryons.

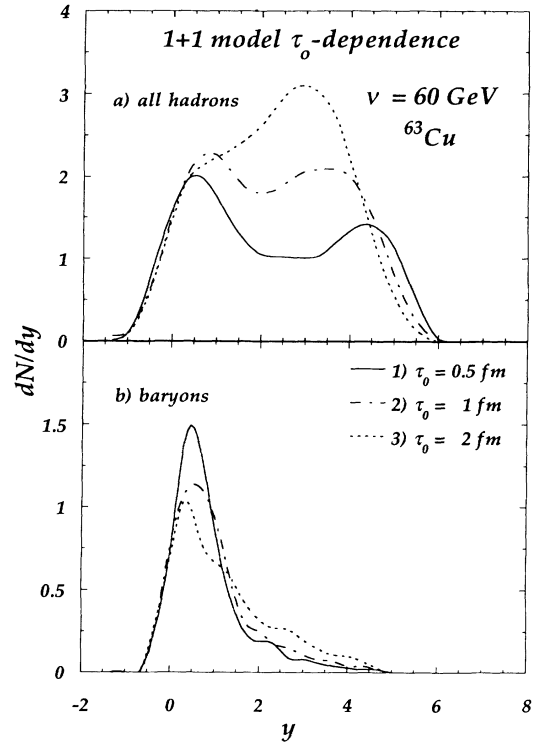


FIG. 5. The τ_0 dependence of the rapidity distributions calculated with the 1+1 model for $A = 63$, $Q^2 = 4$ GeV², and $\kappa = 0.88$ GeV/fm. Calculations were performed with $\tau_0 = 0.5$ fm/c (curve 1), $\tau_0 = 1$ fm/c (curve 2), and $\tau_0 = 2$ fm/c (curve 3), and are shown for (a) all hadrons and (b) all baryons.

and $\kappa = 0.88$ GeV/fm. Although the low rapidity peak remains fairly unchanged with this variation, the total multiplicity substantially increases at $y > 2$ with increasing τ_0 , whereas the baryon peak decreases. We also have varied κ and τ_0 while keeping $\kappa\tau_0 = 0.88$ GeV/c. The results are presented in Fig. 6. We used $\kappa = 0.44, 0.88,$ and 1.76 GeV/fm. The total multiplicity behaves somewhat differently, showing enhancement at low rapidity for larger values of κ , but an unchanged distribution at higher rapidity. The baryon peak remains essentially unchanged, although shifted to slightly lower rapidity. We have also varied κ independently, as shown in Fig. 7, with $\tau_0 = 1.0$ fm/c. The meson multiplicities increase with increasing κ at both low and high rapidity, while the baryon rapidity distribution decreases and is shifted to higher values of rapidity as κ is increased.

In Fig. 8 we show the A dependence ($A = 16, 63, 208$) of the rapidity distributions at fixed $\nu = 60$ GeV and $\sigma_{lq} = 20$ mb. The parameter values used were $\kappa = 0.88$ GeV/fm and $\tau_0 = 1$ fm/c. Note that the high rapidity mesons are not affected as we increase the nuclear size, thus indicating that for this choice of parameters, much of the hadronization occurs outside the nucleus. In Fig. 9 we show the rapidity distribution for ^{63}Cu as a function of σ_{lq} . The number of baryons that participate in the collision increases with increasing σ_{lq} as expected, but the high rapidity meson peak is again unchanged.

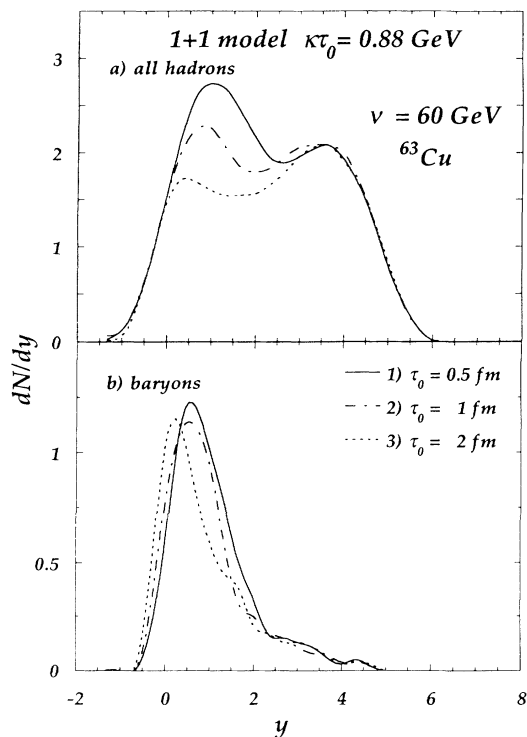


FIG. 6. 1+1 model rapidity distributions are calculated with variations of κ and τ_0 such that $\kappa\tau_0 = 0.88$ GeV. Here $A = 63$, $Q^2 = 4$ GeV². Calculations were performed with $\tau_0 = 0.5$ fm/c (curve 1), $\tau_0 = 1$ fm/c (curve 2), and $\tau_0 = 2$ fm/c (curve 3), and are shown for (a) all hadrons and (b) all baryons.

C. (3+1)-dimensional lepton-nucleus deep-inelastic scattering

The results of the schematic string flip model are qualitatively supported by the (3+1)-dimensional string-parton model simulations. In the present calculations we have chosen $Q^2 > 4$ (GeV/c)² and $0 < x_{Bj} < 1$, at energies $\nu = 7, 20,$ and 40 GeV. The struck nuclear system, ^{63}Cu , is time evolved until all particles have been produced. Interactions of the cascading particles with the nucleus have been allowed for nucleon-nucleon scattering with $\sqrt{s} > 2$ GeV, and nucleon-meson or meson-meson scattering with $\sqrt{s} > 1.6$ GeV. These are natural cut-offs for N - N and π - N inelastic scattering cross sections [21]. In Fig. 10 we show the ν dependence of the rapidity distribution, dN/dy . The effect of intranuclear cascading may be seen near zero rapidity. The initially struck quark string first decays into a baryon and a meson, with the meson carrying the leading quark. The newly formed baryon is at low rapidity and moves through the nucleus, perhaps striking another nucleon as it propagates. We note that the energy of these baryons is small, translating into a small (but nonzero) rapidity.

The effects of the nucleus on the initially struck quark, and subsequent intranuclear cascading, may be investigated in the (3+1)-dimensional model by comparing the rapidity distributions for two cases. We first consider the

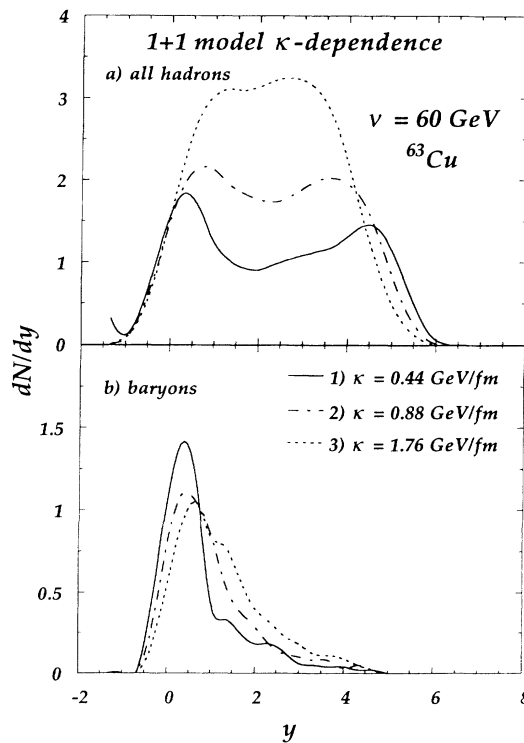


FIG. 7. The κ dependence of the 1+1 model calculated rapidity distributions for $A = 63$, $Q^2 = 4$ GeV², and $\tau_0 = 1.0$ fm/c. Calculations were performed with $\kappa = 0.44$ GeV/fm (curve 1), $\kappa = 0.88$ GeV/fm (curve 2), and $\kappa = 1.76$ GeV/fm (curve 3), and are shown for (a) all hadrons and (b) all baryons.

case where the leading quark is allowed to interact in the nucleus, along with all other cascading interactions. We next investigate the case in which we allow for cascading interactions, but do not allow the leading quark to interact within the nucleus. Finally, we allow for leading quark interactions, but we do not consider the cascading interactions. We present in Fig. 11 the results of these three cases at $\nu = 7$ GeV. In Fig. 11(a) we show the total hadron rapidity distributions with (curve 1) and without (curve 2) leading quark interactions, and with leading quark interactions and no cascading (curve 3). We note that the meson peak is shifted to lower rapidity when leading quark interactions are allowed, and that cascading interactions enhance the low rapidity spectrum. From kinematic considerations at $\nu = 7$ GeV, we find that in the case where the leading quark does not interact, there should be a meson rapidity peak at $y = 1.9$; however, when leading quark interactions are allowed, we see that the nucleus has absorbed energy from the leading quark, thus shifting the meson peak down by roughly 0.5 units of rapidity. Effects of the nucleus may be more vividly seen in Fig. 11(b) in which baryon rapidity distributions are shown. We see that the cascading baryons coming from the nucleus are peaked at very low rapidity ($y = 0.25$), and that they are moving primarily in the forward direction, where the center-of-mass rapidity is calculated to be $y_{c.m.} = 0.1$. Note also that intranuclear cascad-

ing greatly enhances these low rapidity particles. The baryon peak at $y = 1.3$ corresponds to the first baryon in the decay sequence. Allowing for the leading quark to interact within the nucleus gives rise to an enhancement of the peak at $y = 0.25$. As we mentioned, this deposit of the energy of the leading quark into the nucleus causes a shift to lower rapidity for mesons. The leading quark effect has also been studied at $\nu = 20$ GeV, as shown in Fig. 12, where the rapidity shift of the mesons is less pronounced.

We further investigate the effects of the nucleus on the initially struck quark by considering nuclear attenuation of the leading quark. These effects may be calculated by computing the ratio

$$R(\nu) = \frac{\left(\int_{x_f > x_{\min}}^1 dx_f \frac{dN}{dx_f} \right)_{\mu-A}}{\left(\int_{x_f > x_{\min}}^1 dx_f \frac{dN}{dx_f} \right)_{\mu-p}}, \quad (16)$$

which describes the integrated multiplicity in a given range of x_f [22]. We have performed these calculations using the (3+1)-dimensional model, resulting in the ratios $R = 0.69, 0.73, 0.9$, and 0.93 for $\nu = 7$ ($x_f > 0.4$), 11 ($x_f > 0.4$), 20 ($x_f > 0.2$), and 40 ($x_f > 0.2$) GeV,

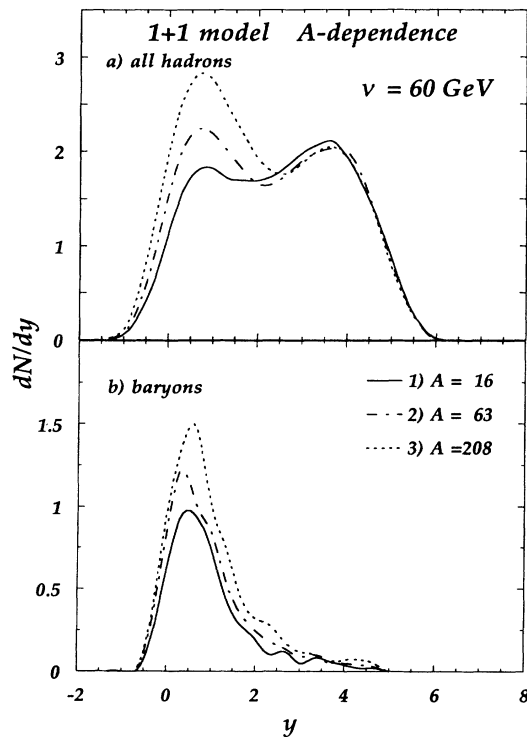


FIG. 8. The A dependence of the 1+1 model calculated rapidity distributions for $\nu = 60$ GeV, $Q^2 = 4$ GeV², $\kappa = 0.88$ GeV/fm, and $\tau_0 = 1.0$ fm/c. Calculations were performed with $A = 16$ (curve 1), $A = 63$ (curve 2), and $A = 208$ (curve 3), and are shown for (a) all hadrons and (b) all baryons.

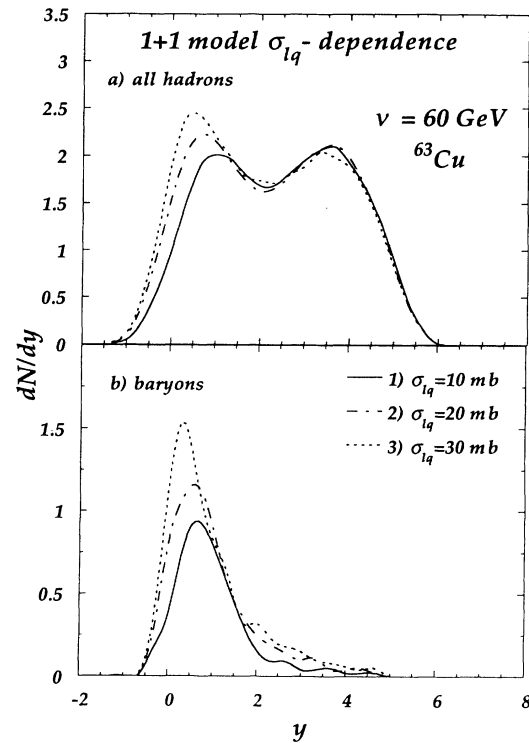


FIG. 9. The σ_{lq} dependence of the 1+1 model calculated rapidity distributions for $Q^2 = 4$ GeV², $A = 63$, $\kappa = 0.88$ GeV/fm, and $\tau_0 = 1.0$ fm/c. Calculations were performed with $\sigma_{lq} = 10$ mb (curve 1), $\sigma_{lq} = 20$ mb (curve 2), and $\sigma_{lq} = 30$ mb (curve 3), and are shown for (a) all hadrons and (b) all baryons.

respectively. These results are commensurate with the 1+1 model calculations. In Fig. 13 we show nuclear attenuation at various energies. Data are taken from Refs. [18, 23, 24]. The (1+1)-dimensional calculations are performed for various values of κ and τ_0 such that $\kappa\tau_0 = 0.88$ GeV. Regardless of the choice of parameters, both models predict an attenuation for $\nu < 20$ GeV. If the leading quark interaction is turned off in the 3+1 model, as discussed in the previous paragraph, then the nuclear attenuation effect is not evident. Therefore, we conclude that the nuclear attenuation at $\nu < 20$ GeV, within the confines of the string models, is primarily due to leading quark effects.

IV. CONCLUSIONS

We have calculated nuclear attenuation of $x_f > 0$ hadrons and nuclear amplification of $x_f < 0$ hadrons produced in deep-inelastic lepton-nucleus collisions. This was done in the framework of Nambu string dynamics which provides a powerful phenomenology for simulating the physics of strongly interacting particles. The (1+1)-dimensional model was used to explore the sensitivity of the predicted phenomena to variations of the model parameters κ , τ_0 , and σ_{lq} over a very wide domain. We have noted that variations in τ_0 and κ dramatically influence the global rapidity distributions. Measurements of the

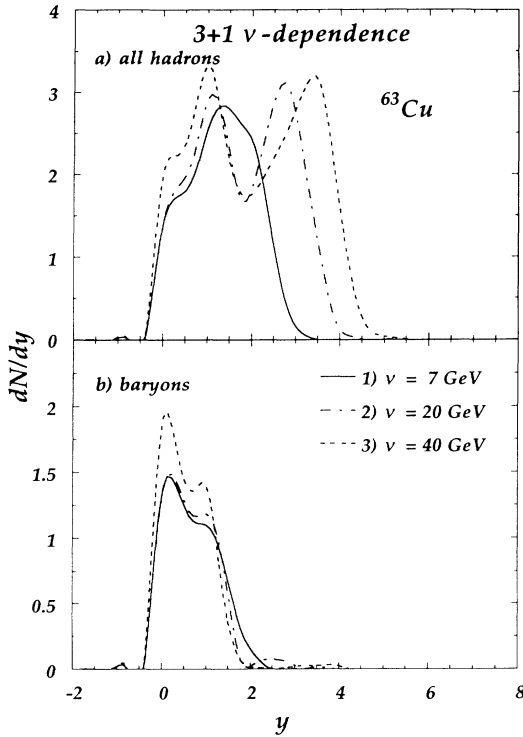


FIG. 10. The ν dependence of the 3+1 model calculated rapidity distributions with $Q^2 > 4$ GeV², $A = 63$, $\tau_0 = 0.5$ fm/c, and $\kappa = 0.88$ GeV/fm. Calculations were performed with $\nu = 7$ GeV (curve 1), 20 GeV (curve 2), and 40 GeV (curve 3), and are shown for (a) all hadrons and (b) all baryons.

full rapidity distribution are needed to fix the parameters. However, comparisons with data should only be taken seriously for the 3+1 version since, as also noted in connection with μ - p data, transverse momentum production is important to account for the width of the x_f distribution.

We have demonstrated that for both models (1+1 and 3+1 strings) the nuclear attenuation effect for $x_f > 0$ is sizable only for $\nu < 20$ GeV, as shown in Fig. 13, in agreement with the limited amount of data available. Unfortunately the nuclear attenuation effects for $x_f > 0$ are rather small and much higher precision data will be needed to draw firmer conclusions. At this stage we can only say that a quark energy loss in nuclear matter, $dE/d\ell \sim 1$ GeV/fm, is compatible with the data. In the future it will be vital to study the systematics in the $x_f < 0$ region since, as seen in Fig. 12, nuclear amplification is much larger there and more sensitive to the combined effects of the leading quark energy loss and secondary cascading. Fortunately, it appears that eventually E665 [24] streamer chamber data may provide a global picture of the full kinematic range.

Knowledge gained from ℓA studies would be very useful for applications of string phenomenology to p - A and A - A reactions. One of the key unsolved questions con-

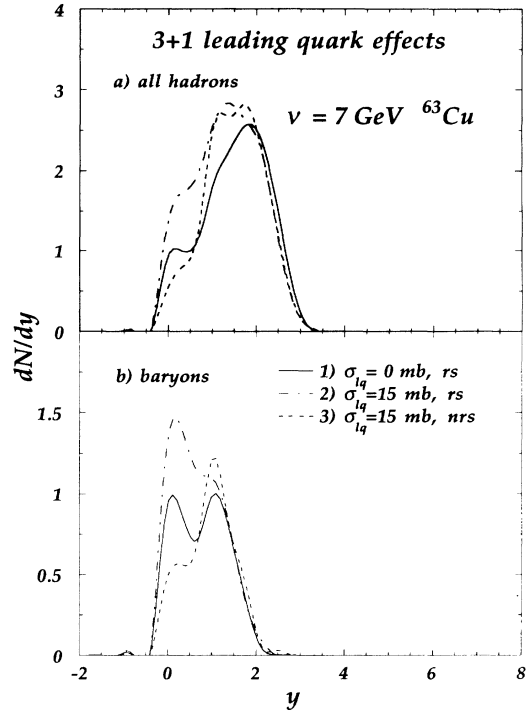
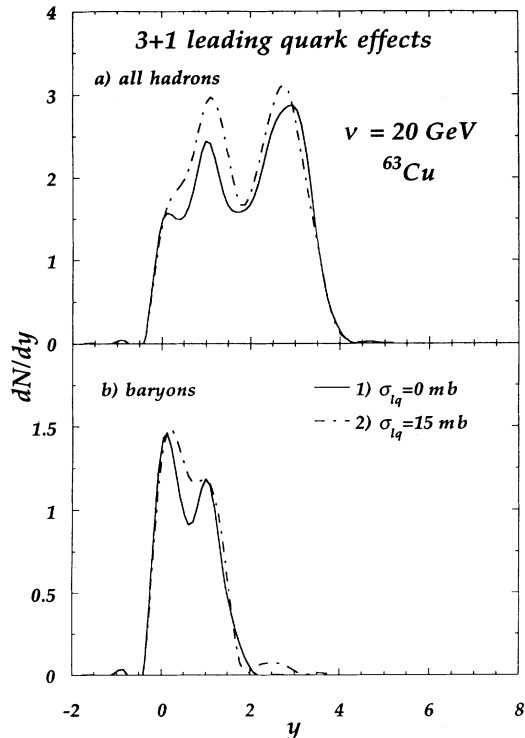


FIG. 11. Rapidity distributions are shown for leading quark effects within the nucleus. Effects of the leading quark, and of cascading particles in the nucleus have been studied in the 3+1 model at $\nu = 7$ GeV, $A = 63$, $Q^2 > 4$ GeV², $\tau_0 = 0.5$ fm/c, and $\kappa = 0.88$ GeV/fm. Calculations were performed with (curve 1) and without (curve 2) leading quark interactions, and with leading quark interactions without intranuclear cascading (curve 3), and are shown for (a) all hadrons and (b) all baryons.

FIG. 12. Same as Fig. 11 but for $\nu = 20 \text{ GeV}$.

cerns the formation zone physics and its influence on secondary cascading. Even though the nuclear attenuation in the $x_f > 0$ region goes away rapidly with $\nu > 20 \text{ GeV}$ [25], there is always a rich nuclear physics in the $x_f < 0$ region from which information on the formation zone physics can be extracted. This is mainly uncharted territory experimentally, and deserves much further emphasis. Nambu string dynamics predicts a wide variety of new nuclear dependent phenomena for hadroproduction. If future ℓA experiments confirm the validity of this phenomenology, the development of hadronic transport theory needed especially for applications to A - A would be greatly simplified [8].

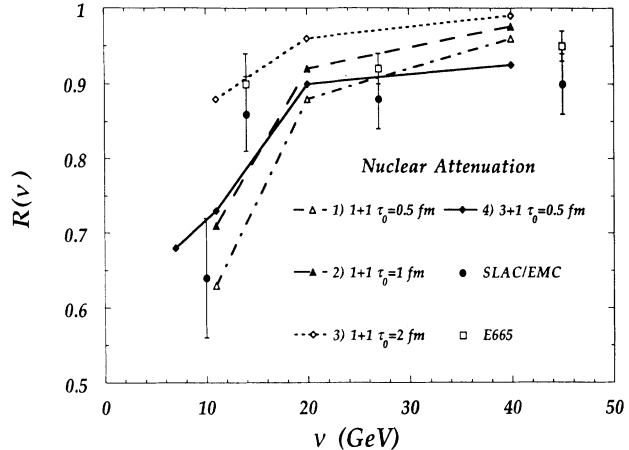


FIG. 13. The nuclear attenuation ratio R as a function of ν is presented for the ^{63}Cu nucleus. Calculations were performed in the 1+1 model for various choices of κ such that $\kappa\tau_0 = 0.88 \text{ GeV}$, and $Q^2 = 4 \text{ GeV}^2$, for $\kappa = 1.76 \text{ GeV/fm}$ (curve 1), $\kappa = 0.88 \text{ GeV/fm}$ (curve 2), and $\kappa = 0.44 \text{ GeV/fm}$ (curve 3). The attenuation is also measured in the 3+1 model for $\kappa\tau_0 = 0.88 \text{ GeV/c}$ (curve 4). Experimental measurements are taken from Refs. [18, 23] (SLAC,ECM) and Ref. [24] (E665).

ACKNOWLEDGMENTS

This research was sponsored in part by the U.S. Department of Energy under Contract No. DE-AC05-84OR21400 with Martin Marietta Energy Systems, Inc., under Grant No. DE-FG05-87ER40376 with Vanderbilt University, under Grant No. DE-FG05-90ER40592 with Duke University, and under Contract No. DE-AC03-765F00098 with Lawrence Berkeley Laboratory. The numerical calculations were carried out on the Intel iPSC/860 hypercube at the Oak Ridge National Laboratory. The authors also wish to acknowledge the Institute for Nuclear Theory at the University of Washington where some of the development of the present work took place.

- [1] *Proceedings of the Conference on Electronuclear Physics with Internal Targets*, 1989, edited by R. Arnold (World Scientific, Singapore, 1990), pp. 1–303.
- [2] X. Artru, *Acta Phys. Pol. B* **17**, 457 (1986); *Phys. Rep.* **97**, 147 (1983).
- [3] B. Andersson, G. Gustafson, G. Ingelman, and T. Sjöstrand, *Phys. Rep.* **97**, 33 (1983); B. Andersson and G. Gustafson, *Z. Phys. C* **3**, 223 (1980).
- [4] G. Ingelman, "LEPTO version 4.3," CERN library long writeup THE LUND MONTE CARLO PROGRAMS (April 1987).
- [5] T. Gotō, *Prog. Theor. Phys.* **46**, 1560 (1971); P. Goddard, J. Goldstone, C. Rebbi, and C. B. Thorn, *Nucl. Phys.* **B56**, 109 (1973).
- [6] K. Sailer, B. Müller, and W. Greiner, *J. Mod. Phys. A*

- 4**, 437 (1989); K. Sailer, B. Müller, and W. Greiner, in *Proceedings of the Nuclear Equation of State*, edited by W. Greiner and H. Stöcker (Plenum, New York, 1990), p. 531.
- [7] E. A. Remler, in *Proceedings of the International Workshop on Quark-Gluon Structure of Hadrons and Nuclei*, Shanghai, 1990 (unpublished); E. A. Remler, William & Mary report, 1988 (unpublished).
- [8] D. J. Dean, A. S. Umar, J.-S. Wu, and M. R. Strayer, *Phys. Rev. C* **45**, 400 (1992); D. J. Dean, A. S. Umar, J.-S. Wu, and M. R. Strayer, in *Computational Quantum Physics*, AIP Conf. Proc. 260, edited by A. S. Umar, V. E. Oberacker, M. R. Strayer, and C. Bottcher (AIP, New York, 1992); D. J. Dean, Ph.D. thesis, Vanderbilt University, 1991 (unpublished).

- [9] X. N. Wang and M. Gyulassy, Phys. Rev. D **44**, 3501 (1991); **45**, 844 (1992).
- [10] M. Gyulassy and M. Plümer, Nucl. Phys. **B346**, 1 (1990).
- [11] A. Bialas and M. Gyulassy, Nucl. Phys. **B291**, 793 (1987).
- [12] J. K. Gunion and G. F. Bertsch, Phys. Rev. D **25**, 746 (1982).
- [13] F. Niedermayer, Phys. Rev. D **34**, 3494 (1986).
- [14] E. L. Feinberg, Zh. Eksp. Teor. Fiz. **50**, 202 (1966) [Sov. Phys. JETP **23**, 132 (1966)]; N.N. Nikolaev, Usp. Fiz. Nauk. **134**, 369 (1981) [Sov. Phys. Usp. **24**, 531 (1981)].
- [15] M. Gyulassy *et al.*, in *Intersections Between Particle and Nuclear Physics*, AIP Conf. Proc. No. 243, edited by W. T. H. van Oers (AIP, New York, 1992), p. 224; Lawrence Berkley Laboratory Report No. LBL-31003, 1992 (unpublished).
- [16] G. T. Bodwin, S. J. Brodsky, and G.P. Lepage, Phys. Rev. D **39**, 3287 (1989).
- [17] *Perturbative Quantum Chromodynamics*, edited by A.H. Mueller, Advanced Series on Directions of High Energy Physics Vol. 5 (World Scientific, Singapore, 1989).
- [18] L. S. Osborne *et al.*, Phys. Rev. Lett. **40**, 1624 (1978).
- [19] X. Artru and G. Mennessier, Nucl. Phys. **B70**, 93 (1974).
- [20] M. Arneodo *et al.*, Phys. Lett. **150B**, 458 (1985); M. Arneodo *et al.*, Z. Phys. C **35**, 417 (1987).
- [21] M. Aguilar-Benitez *et al.*, Phys. Lett. **170B**, 1 (1986).
- [22] A. Arvidson *et al.*, Nucl. Phys. **B246**, 381 (1984).
- [23] P. B. Renton, EMC Collaboration, in *Intersections Between Particle and Nuclear Physics*, Proceedings of the Conference, Rockport, ME, May 14–19, 1988, AIP Conf. Proc. No. 176, edited by G. M. Bunce (AIP, New York, 1988), p. 502.
- [24] A.F. Salvarani, E665 Collaboration, Ph.D. thesis, UCSD, 1991; V. Papavassiliou, SLAC Report No. SLAC-392, 1992.
- [25] M. G. Abreu *et al.*, Z. Phys. C **25**, 115 (1984).